AMERICAN SOCIETY FOR MICROBIOLOGY | Journal of Virology

Host-Microbial Interactions | Full-Length Text

Inhibition of the RLR signaling pathway by SARS-CoV-2 ORF7b is mediated by MAVS and abrogated by ORF7b-homologous interfering peptide

Xiao Xiao,[1,2,3] Yanan Fu,[1,2] Wanling You,[1,2] Congcong Huang,[1,2,3] Feng Zeng,[1,2] Xinsheng Gu,[1] Xiaoguang Sun,[1,2] Jian Li,[1,2] Qiwei Zhang,[4] Weixing Du,[1] Gong Cheng,[5] Zhixin Liu,[1,2,3] Long Liu[1,2,3]

AUTHOR AFFILIATIONS See affiliation list on p. 18.

ABSTRACT Coronavirus disease 2019 (COVID-19) is caused by severe acute respiratory syndrome coronavirus 2 (SARS-CoV-2) infection and characterized by dysregulated immune response. Studies have shown that the SARS-CoV-2 accessory protein ORF7b induces host cell apoptosis through the tumor necrosis factor alpha (TNF-α) pathway and blocks the production of interferon beta (IFN-β). The underlying mechanism remains to be investigated. In this study, we found that ORF7b facilitated viral infection and production, and inhibited the RIG-I-like receptor (RLR) signaling pathway through selectively interacting with mitochondrial antiviral-signaling protein (MAVS). $MAVS_{439-466}$ region and MAVS Lys461 were essential for the physical association between MAVS and ORF7b, and the inhibition of the RLR signaling pathway by ORF7b. $MAVS_{K461}$/K63 ubiquitination was essential for the RLR signaling regulated by the MAVS–ORF7b complex. ORF7b interfered with the recruitment of tumor necrosis factor receptor-related factor 6 (TRAF6) and the activation of the RLR signaling pathway by MAVS. Furthermore, interfering peptides targeting the ORF7b complex reversed the ORF7b-suppressed MAVS-RLR signaling pathway. The most potent interfering peptide V disrupts the formation of ORF7b tetramers, reverses the levels of the ORF7b-inhibited physical association between MAVS and TRAF6, leading to the suppression of viral growth and infection. Overall, this study provides a mechanism for the suppression of innate immunity by SARS-CoV-2 infection and the mechanism-based approach via interfering peptides to potentially prevent SARS-CoV-2 infection.

IMPORTANCE The pandemic coronavirus disease 2019 (COVID-19) is caused by severe acute respiratory syndrome coronavirus 2 (SARS-CoV-2) infection and continues to be a threat to public health. It is imperative to understand the biology of SARS-CoV-2 infection and find approaches to prevent SARS-CoV-2 infection and ameliorate COVID-19. Multiple SARS-CoV-2 proteins are known to function on the innate immune response, but the underlying mechanism remains unknown. This study shows that ORF7b inhibits the RIG-I-like receptor (RLR) signaling pathway through the physical association between ORF7b and mitochondrial antiviral-signaling protein (MAVS), impairing the K63-linked MAVS polyubiquitination and its recruitment of tumor necrosis factor receptor-related factor 6 (TRAF6) to MAVS. The most potent interfering peptide V targeting the ORF7b–MAVS complex may reverse the suppression of the MAVS-mediated RLR signaling pathway by ORF7b and prevent viral infection and production. This study may provide new insights into the pathogenic mechanism of SARS-CoV-2 and a strategy to develop new drugs to prevent SARS-CoV-2 infection.

KEYWORDS SARS-CoV-2, ORF7b, MAVS, RLR signaling pathway, interfering peptide

Editor Stacey Schultz-Cherry, St. Jude Children's Research Hospital, Memphis, Tennessee, USA

Address correspondence to Long Liu, liulong2015@outlook.com, Zhixin Liu, lzx20022456@126.com, Gong Cheng, gongcheng@mail.tsinghua.edu.cn, or Weixing Du, duwx-025@163.com.

Xiao Xiao, Yanan Fu, and Wanling You contributed equally to this article. Author order was determined based on their contribution to the article.

The authors declare no conflict of interest.

See the funding table on p. 18.

Received 9 October 2023
Accepted 15 March 2024
Published 4 April 2024

Coronavirus disease 2019 (COVID-19), which is caused by severe acute respiratory syndrome coronavirus 2 (SARS-CoV-2) infection, continues to be a significant health concern worldwide (1, 2). As of 11 February 2024, more than 774 million people have been affected and 7.03 million cumulative deaths have been caused (https://covid19.who.int). It is imperative to understand the biology of SARS-CoV-2 infection and find approaches to prevent and ameliorate COVID-19. The coronavirus SARS-CoV-2 is a single-stranded positive-sense RNA virus found in several animal species (3). The genome of SARS-CoV-2 encodes more than 28 proteins for viral assembly and functions, including 4 structural proteins, 16 non-structural proteins, and 8 accessory proteins (4). After angiotensin-converting enzyme 2 (ACE2)-mediated entrance (5), SARS-CoV-2 virus produces non-structural, structural, and accessory proteins and reproduces through genome replication, transcription, viral assembly, and release from host cells (6). SARS-CoV-2 infection also perturbs the immune system by suppressing type I responses and enhancing the proinflammatory response, promoting viral replication and host tissue damage (7–10). The significant feature of SARS-CoV-2 infection is that the levels of type I interferon (IFN) are extremely low (10).

The host innate immune response is one of the first lines of defense against viral infection (11). Upon recognition of viral dsRNA, the viral RNA sensor RIG-I-like receptor (RLRs) bind with mitochondrial antiviral-signaling protein (MAVS) through K63-linked ubiquitination and their caspase recruitment domains (CARDs) (12). Subsequently, the MAVS rapidly forms prion-like aggregates through CARDs, binds with the tumor necrosis factor receptor-related factors (TRAFs) 2,5,6 via its proline-rich region (PRR) domain, and then activates IKK and TBK1. Upon activation, the cytosolic kinase TBK1 promotes the phosphorylation and homodimerization of IRF3, which induces the transcription of type I IFNs. The cytosolic kinase IKK activates NF-κB to promote the transcription of proinflammatory cytokines, including tumor necrosis factor alpha (TNF-α) (13–15). SARS-CoV accessory protein ORF9b localizes in mitochondria and directly manipulates mitochondrial function to evade host cell immunity and facilitate virus replication and disease (16). Upon SARS-CoV-2 infection, ORF9b protein inhibits the IFN-I pathway by interacting with MAVS and preventing the phosphorylation and nuclear translocation of IRF3 (17). ORF9b inhibits the binding between hTOM70 and Hsp90, which undermines the recruitment of Hsp90 to TBK1/IRF3, thus weakening the signaling cascade for the IFN-I pathway (18, 19). ORF10 inhibits the IFN-I pathway by inducing mitophagy-mediated degradation of MAVS (20). The localization of SARS-CoV-2 proteins in mitochondria may play critical roles in the pathogenesis of COVID-19, activating inflammasome and suppressing the innate and adaptive immunity after viral infection (21).

The SARS-CoV-2 accessory protein ORF7b encodes 43 amino acid residues, including a fully conserved transmembrane domain (22). ORF7b may be involved in cellular infection processes of SARS-CoV-2 (23). Recently, studies in our lab and by other groups have shown that SARS-CoV-2 ORF7b induces host cell apoptosis through the TNF-α pathway and blocks the production of IFN-β (24, 25). We hypothesized that ORF7b interferes with the upstream of the RLR signaling pathways and thus blocks TNF-α and IFN-β production.

Increasing evidence suggests that peptide drugs targeting disease-relevant protein–protein interactions could be key factors in clinical success (26). Interfering peptides targeting the SARS-CoV-2 nuclear coat protein dimer structure have been designed to disrupt the liquid–liquid phase separation (LLPS) of SARS-CoV-2-NP, thereby enhancing the intrinsic antiviral response of the host *in vitro* and *in vivo* (27). Interfering peptides targeting the ORF7b may prevent infection and production of SARS-CoV-2 and reverse the suppression of innate immunity by ORF7b.

In this study, we investigated the mechanism of inhibition of the RLR signaling pathway by ORF7b and developed interfering peptides targeting the ORF7b to prevent SARS-CoV-2 infection and innate immunity compromise. We found that ORF7b specifically binds to MAVS, impairing the K63-linked MAVS polyubiquitination and its recruitment of downstream adaptors and resulting in inhibiting the RLR signaling

pathway. We also identified interfering peptides that targeted the ORF7b–MAVS complex and reversed the suppression of the MAVS-mediated RLR signaling pathway by ORF7b, preventing viral infection and growth. Our study may provide new insights into the pathogenic mechanism of SARS-CoV-2 and a strategy to develop new drugs to prevent SARS-CoV-2 infection.

RESULTS

SARS-CoV-2 accessory protein ORF7b facilitated viral infection and production, and inhibited the RLR signaling pathway

To investigate the role of ORF7b in viral infection and production, we transfected HEK293T cells with pCAGGS-ORF7b-FLAG or empty vector (pCAGGS) and pMD2G, and then infected the cells with VSV-ΔG-GFP and determined the infection and production of VSV-ΔG-GFP. The results showed that GFP was expressed in the HEK293T cells infected with VSV-ΔG-GFP as determined by fluorescence microscopy (Fig. 1A) and Western blotting (Fig. 1B), suggesting that the production of viral VSV-ΔG-GFP was present in the HEK293T cells. Overexpression of ORF7b-FLAG resulted in enhanced VSV-ΔG-GFP production, compared with the control (Fig. 1A and B). Furthermore, the flow cytometry results confirmed the presence of GFP-expressing HEK293T cells after VSV-ΔG-GFP infection (Fig. 1C) and showed that overexpression of ORF7b-FLAG resulted in increase in the rate of GFP-positive HEK293T cells, compared with the control (Fig. 1C and D). The viral VSV-ΔG-GFP titer was significantly increased by overexpression of ORF7b-FLAG (Fig. 1E). These results suggested that ORF7b enhanced the infection and production of viral VSV-ΔG-GFP in the HEK293T cells.

Previous proteomic study indicates that there is a functional association between ORF7b and MAVS (28), suggesting that ORF7b affects the innate immune function. To examine the potential effect of ORF7b on the innate immune function, we transfected HEK293T cells and HEK293T-ORF7b-GFP cells, which stably expressed ORF7b-GFP, with IFN-β-pGL3, pRL-SV40, RLR signaling components RIG-I, MDA5, MAVS, TBK1 expression plasmids, and the control mock plasmid (pCMV-Flag), followed by poly (I:C) treatment. We determined the relative luciferase activity, which indicates the IFN-β promoter activity. The results showed that the IFN-β promoter was significantly activated in the HEK293T cells and HEK293T-ORF7b-GFP cells transfected with RIG-I, MDA5, MAVS, and TBK1 plasmids, compared with the mock control group (Fig. 1G). The magnitudes of activation of the IFN-β promoter by RIG-I, MDA5, MAVS, and TBK1 in the HEK293T-ORF7b-GFP cells were significantly lower (by RIG-I, MDA5, MAVS) or tended to be lower (by TBK1) than those in the HEK293T cells (Fig. 1G). These results suggested that ORF7b inhibited the RLR signaling pathway.

ORF7b was physically associated with MAVS, and $MAVS_{439-466}$ region was essential for this association

To investigate the potential mechanism underlying the inhibition of the RLR signaling pathway by ORF7b, we transfected HEK293T-ORF7b-GFP cells with RIG-I, MDA5, MAVS, and TBK1 expression plasmids, and treated the cells with poly (I:C). We examined whether ORF7b formed complexes with RIG-I, MDA5, MAVS, and TBK1 in the HEK293T cells using co-immunoprecipitation (co-IP) assays. The results indicated that ORF7b was physically associated with MAVS but not with RIG-I, MDA5, or TBK1 in the HEK293T cells (Fig. 2A).

MAVS is a 540-amino acid protein that contains three domains: N-terminal CARD, middle PRR, and C-terminal transmembrane (TM) domain (29). To further investigate the specific domain/region of MAVS responsible for the physical association between ORF7b and MAVS, we transfected HEK293T-ORF7b-GFP cells with plasmids encoding MAVS and its truncations (Fig. 2B), and performed co-IP assays. The results indicated that ORF7b was associated with MAVS, $MAVS_{181-541}$, $MAVS_{362-541}$, and $MAVS_{1-90,439-541}$, but not with the truncates $MAVS_{1-180}$, $MAVS_{1-438}$, or $MAVS_{1-90,467-541}$ (Fig. 2C). Therefore, the $MAVS_{439-466}$ domain was required for MAVS to interact with ORF7b.

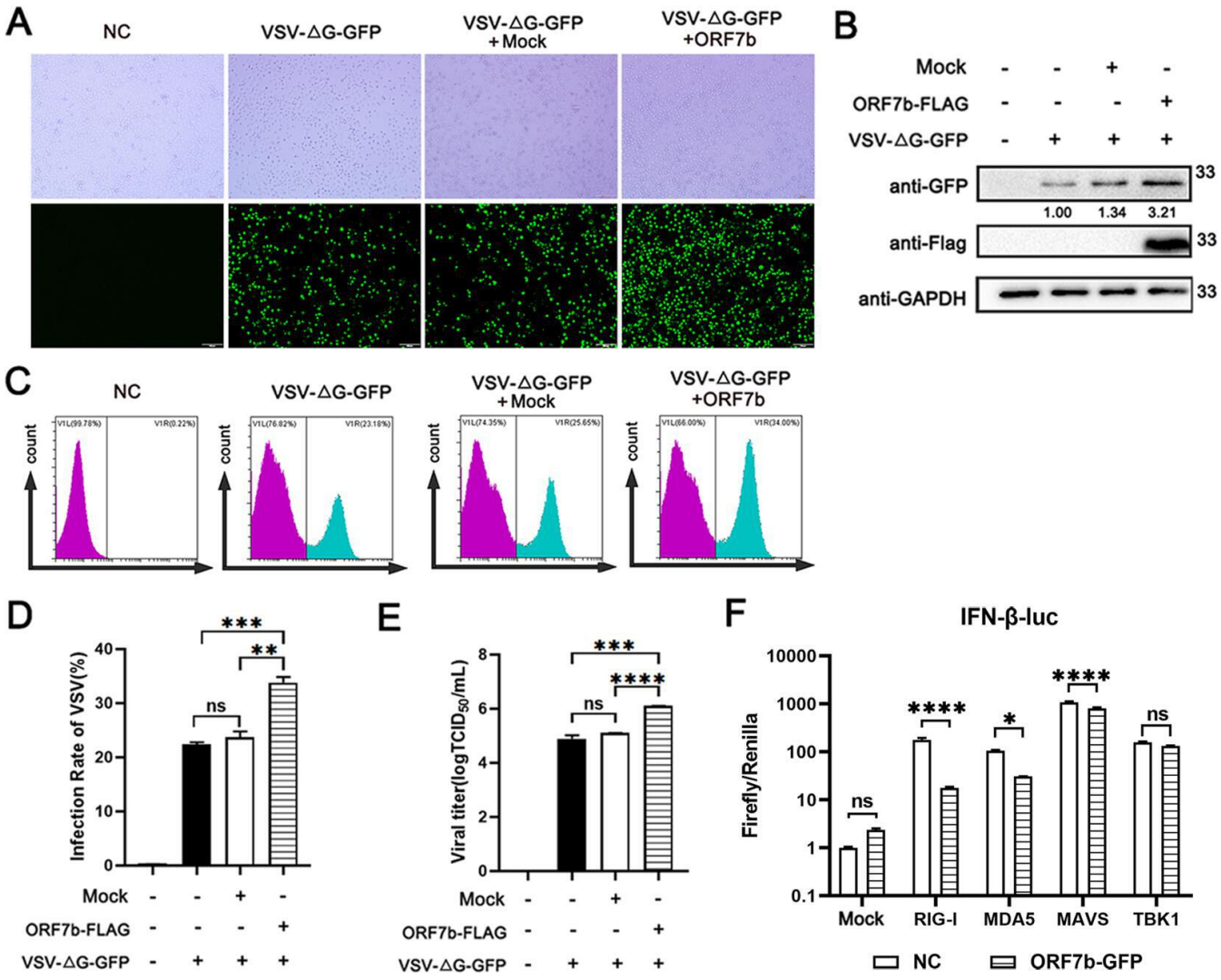

FIG 1 SARS-CoV-2 accessory protein ORF7b facilitated viral infection and production, and inhibited the RLR pathway-mediated IFN-β promoter activity in HEK293T cells. (A–E) ORF7b facilitated viral infection and production. The HEK293T cells were co-transfected with pCAGGS-ORF7b-FLAG or pCAGGS plasmids and pMD2G. Twenty-four hours later, the cells were infected with VSV-ΔG-GFP for 1 h and then incubated for 12 h. The cells and media were subjected to subsequent examination. (A, B) ORF7b enhanced GFP expression in the HEK293T cells infected with VSV-ΔG-GFP. GFP expression was observed and photographed using a fluorescence microscope (A) and was determined using Western blotting (B). (C, D) ORF7b enhanced the viral infection of VSV-ΔG-GFP in the HEK293T cells. The GFP-positive cells were identified using the flow cytometry assay (C). Infection rate was calculated according to the result of the flow cytometry assay (D). (E) ORF7b enhanced the viral production in the HEK293T cells infected with VSV-ΔG-GFP. Viral titers in the media were determined using the Spearman-Karber method. (F) ORF7b inhibited the RLR pathway-mediated IFN-β promoter activity. The HEK293T cells and HEK293T-ORF7b-GFP cells, which stably expressed ORF7b-GFP, were transfected with IFN-β-pGL3, pRL-SV40, and the RIG-I, MDA5, MAVS, TBK1 expression plasmids or control mock plasmid (pCMV-Flag) for 18 h, followed by 10 μg/mL poly (I:C) treatment for 6 h. Relative luciferase activity, which indicates the IFN-β promoter activity, was determined. *$P < 0.05$, **$P < 0.01$, ***$<I>P < 0.001$, and ****$<I>P < 0.0001$; Student's *t*-test or one-way ANOVA, Tukey's post-hoc test. NC, negative control. ns, no significant difference.

Furthermore, the confocal microscopy results showed that ORF7b was fully co-localized with full-length MAVS, $MAVS_{1-180}$, $MAVS_{1-438}$, $MAVS_{181-541}$, $MAVS_{362-541}$, and $MAVS_{1-90,439-541}$, and partially co-localized with $MAVS_{91-180,467-541}$, but not with $MAVS_{1-90,467-541}$ (Fig. 2D). Pearson's correlation coefficient (PCC) (Fig. 2D) indicates the extent of co-localization of the two fluorescence signals (30). These results suggested that $MAVS_{439-466}$ was essential for the co-localization of MAVS and ORF7b. Therefore, ORF7b was physically associated with MAVS, and $MAVS_{439-466}$ region was essential for this association.

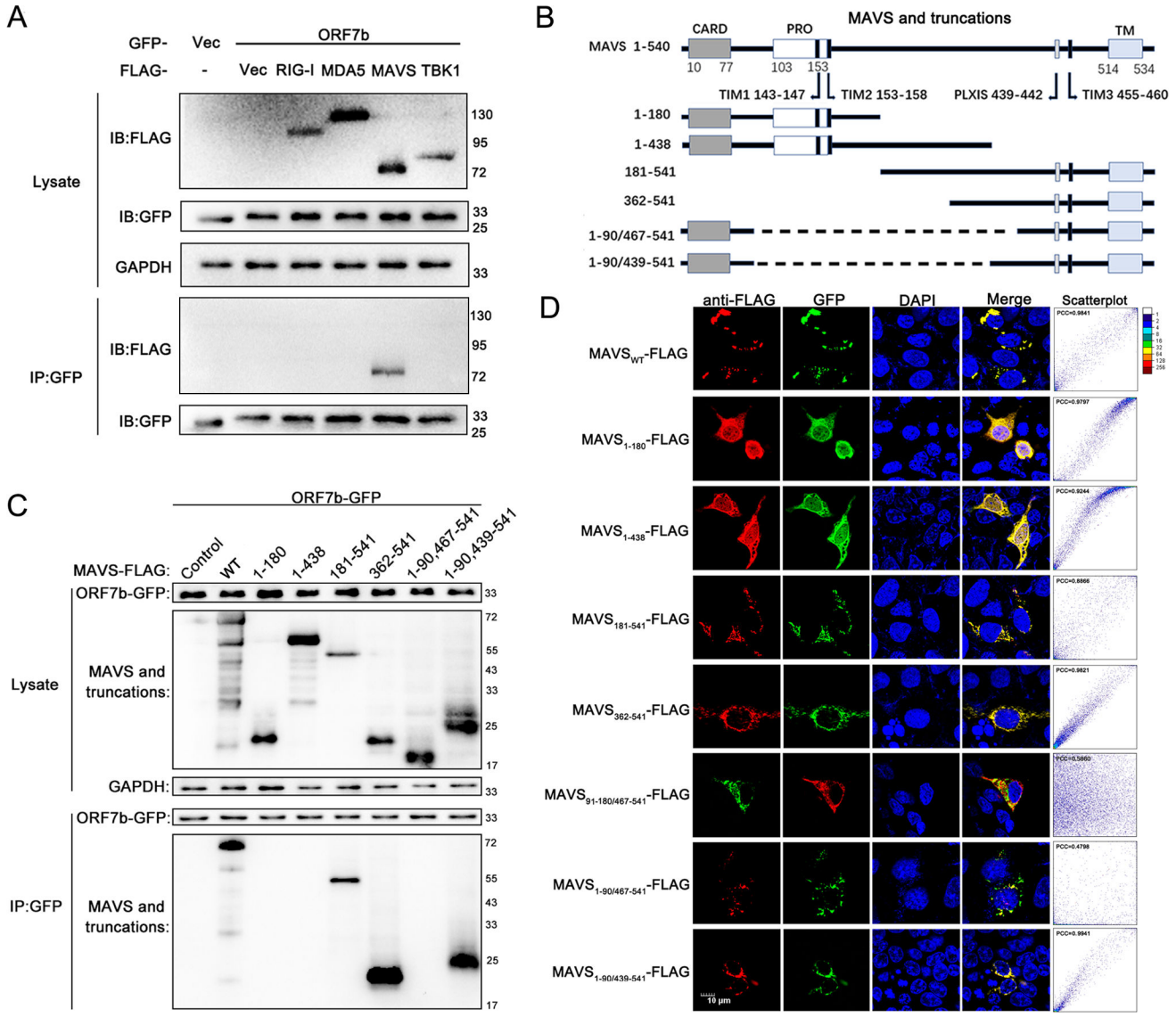

FIG 2 ORF7b was physically associated with MAVS, and MAVS$_{439-466}$ region was essential for this association. (A) ORF7b was physically associated with MAVS. HEK293T-ORF7b-GFP cells were transfected with RIG-I, MDA5, MAVS, TBK1 expression plasmids, and the respective control vectors for 18 h, and then treated with poly (I:C) for 6 h. The cells were collected and subjected to co-IP assays using the anti-GFP magnetic beads. The control vector expressing GFP alone in HEK293T was used as the control group. (B) Schematic domains/regions of the full-length MAVS and its truncation mutants. (C) MAVS$_{439-466}$ region was essential for the physical association between ORF7b and MAVS. The HEK293T-ORF7b-GFP cells were transfected with plasmids encoding MAVS and its truncations MAVS$_{1-180}$-FLAG, MAVS$_{181-541}$-FLAG, MAVS$_{1-90,467-541}$-FLAG, MAVS$_{362-541}$-FLAG, MAVS$_{1-438}$-FLAG, and MAVS$_{1-90,439-541}$-FLAG for 18 h, and then treated with 10 μg/mL poly (I:C) for 6 h. The cells were collected and subjected to co-IP assays using the anti-GFP magnetic beads. The empty vector expressing GFP alone in HEK293T was used as the control group. (D) Subcellular co-localization analysis of ORF7b with MAVS and its truncations. The HEK293T-ORF7b-GFP cells were transfected with plasmids encoding MAVS and its truncations for 18 h, and then treated with poly (I:C) for 6 h. The cells were subjected to immunocytochemistry and confocal microscopy analysis using Alexa-Fluor-555-conjugated goat anti-rabbit IgG secondary antibody (anti-flag, red). Pearson's correlation coefficients indicating the extent of co-localization of the two fluorescence signals were calculated. Scale bars, 10 μm.

MAVS Lys461 was essential for physical association between MAVS and ORF7b, and for inhibition of the RLR signaling pathway by ORF7b

Studies have shown that several key amino acid residues in the MAVS$_{439-466}$ region play essential roles in the RLR signaling pathway. Ser442 is essential for IRF3 binding and activation (31), Glu457 is essential for MAVS to interact with TRAF6 and mediates the activation of NF-κB and IRF3 pathways (32), and Lys461 promotes K63-linked polyubiquitination, which facilitates the formation of prion-like MAVS aggregates (33).

To investigate whether these amino acid residues play essential roles in the interaction between MAVS and ORF7b, we transfected HEK293T-ORF7b-GFP cells with MAVS, $MAVS_{S442A}$, $MAVS_{E457D}$, and $MAVS_{K461R}$ expression plasmids, treated the cells with poly (I:C), and performed co-IP assays. The results showed that the amounts of $MAVS_{E457D}$ and $MAVS_{K461R}$ proteins precipitated by ORF7b were less than those of MAVS and $MAVS_{S442A}$. The reduction in the amount of $MAVS_{K461R}$ protein was dramatic (Fig. 3A). The results suggested that MAVS Lys461 was essential for the physical association between MAVS and ORF7b.

To investigate whether Ser442, Glu457, and Lys461 play essential roles in the inhibition of the MAVS-mediated IFN-β promoter activity by ORF7b, we transfected HEK293T cells and HEK293T-ORF7b-GFP cells with IFN-β-pGL3, pRL-SV40, MAVS, $MAVS_{S442A}$, $MAVS_{E457D}$, $MAVS_{K461R}$ expression plasmids, and the control plasmid, followed by poly (I:C) treatment. We determined the relative luciferase activity, which indicates the IFN-β promoter activity. The results showed that the IFN-β promoter activity was significantly activated by MAVS, $MAVS_{S442A}$, $MAVS_{E457D}$, and $MAVS_{K461R}$ (Fig. 3B). The magnitudes of activation by $MAVS_{S442A}$, $MAVS_{E457D}$, and $MAVS_{K461R}$ were

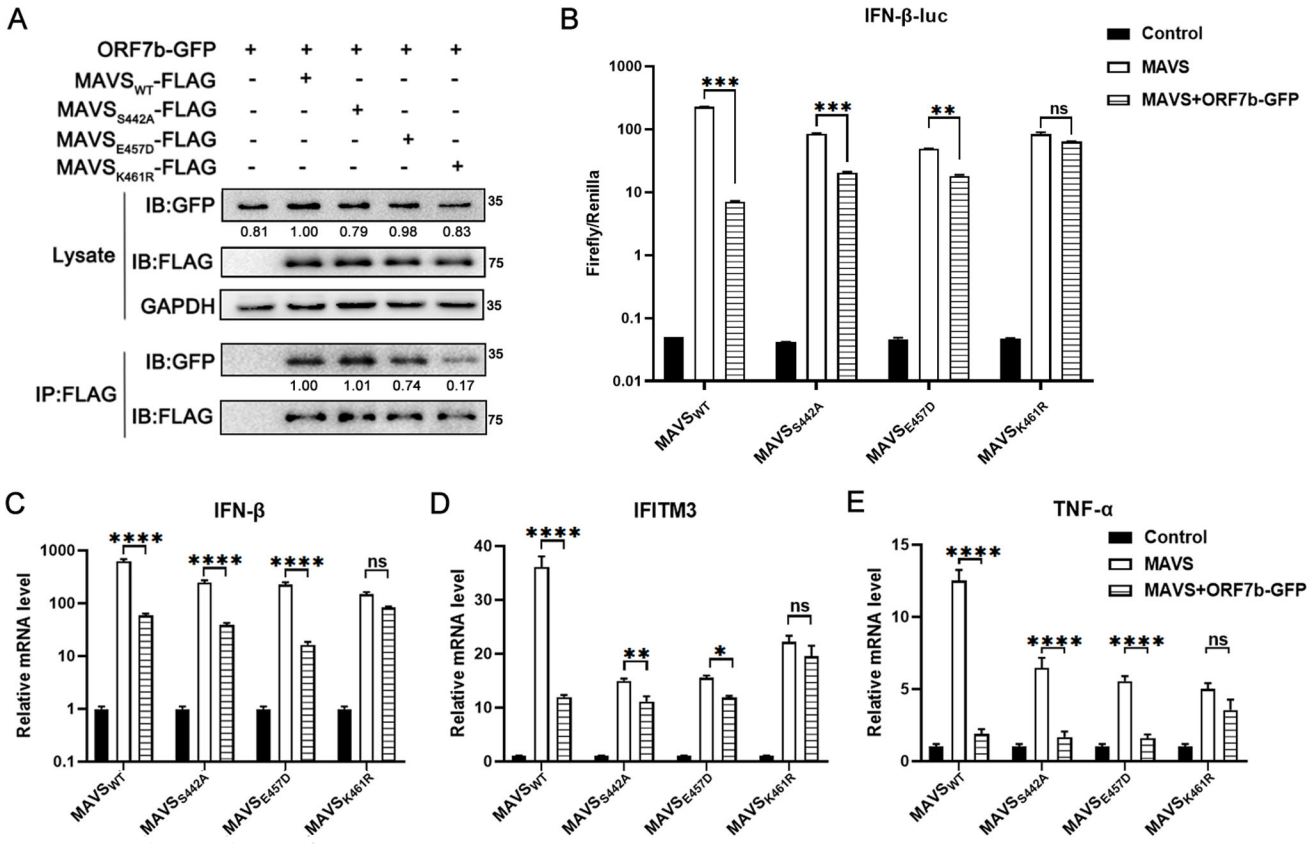

FIG 3 MAVS Lys461 was essential for physical association between MAVS and ORF7b, and for inhibition of the RLR signaling pathway by ORF7b. (A) MAVS Lys461 was essential for physical association between MAVS and ORF7b. HEK293T-ORF7b-GFP cells were transfected with MAVS, $MAVS_{S442A}$, $MAVS_{E457D}$, and $MAVS_{K461R}$ expression plasmids for 18 h, and treated with 10 µg/mL poly (I:C) for 6 h. The cells were collected, and co-IP assays were performed. (B) MAVS Lys461 was essential for inhibition of the MAVS-mediated IFN-β promoter activity by ORF7b. Luciferase-based IFN-β promoter activity was detected in the HEK293T cells and HEK293T-ORF7b-GFP cells. The cells were co-transfected with reporter plasmids and a plasmid expressing wild-type MAVS or its mutants, followed by stimulation with poly (I:C). The HEK293T cells and HEK293T-ORF7b-GFP cells were transfected with IFN-β-pGL3, pRL-SV40, MAVS, MAVSS442A, MAVSE457D, MAVSK461R expression plasmids, and the control plasmid for 18 h, followed by 10 µg/mL poly (I:C) treatment for 6 h. The relative luciferase activity was determined. (C–E) MAVS Lys461 was essential for inhibition of the IFN-β signal pathway and TNF-α expression by ORF7b. The HEK293T cells and HEK293T-ORF7b-GFP cells were transfected with MAVS, $MAVS_{S442A}$, $MAVS_{E457D}$, $MAVS_{K461R}$ expression plasmids, and the control plasmid for 18 h, followed by 10 µg/mL poly (I:C) treatment for 6 h. *IFN-β* (C), *IFITM3* (D), and *TNF-α* (E) mRNA levels were determined using qPCR. *$P < 0.05$, **$<I>P < 0.01$, ***$<I>P < 0.001$, and ****$<I>P < 0.0001$; ns, no significant difference, Student's *t*-test.

significantly lower than that by MAVS (Fig. 3B), suggesting that Ser442, Glu457, and Lys461 were essential for MAVS-mediated IFN-β promoter activity. Furthermore, the IFN-β promoter activity activated by MAVS, $MAVS_{S442A}$, and $MAVS_{E457D}$, but not by $MAVS_{K461R}$, was significantly inhibited by ORF7b (Fig. 3B), suggesting that MAVS Lys461 was essential for the inhibition of the MAVS-mediated IFN-β promoter activity by ORF7b.

To investigate whether Ser442, Glu457, and Lys461 play essential roles in the inhibition of the MAVS-mediated RLR signal pathway by ORF7b, we transfected HEK293T cells and HEK293T-ORF7b-GFP cells with MAVS, $MAVS_{S442A}$, $MAVS_{E457D}$, $MAVS_{K461R}$ expression plasmids, and the control plasmid, and treated the cells with poly (I:C). We determined the *IFN-β*, *IFITM3*, and *TNF-α* mRNA levels with quantitative PCR (qPCR). The results showed that *IFN-β*, *IFITM3*, and *TNF-α* mRNA expression was significantly activated by MAVS, $MAVS_{S442A}$, $MAVS_{E457D}$, and $MAVS_{K461R}$ (Fig. 3C through E). The magnitudes of activation by $MAVS_{S442A}$, $MAVS_{E457D}$, and $MAVS_{K461R}$ were significantly lower than that by MAVS (Fig. 3C through E), suggesting that Ser442, Glu457, and Lys461 were essential for the MAVS-mediated *IFN-β*, *IFITM3*, and *TNF-α* mRNA expression. Furthermore, the *IFN-β*, *IFITM3*, and *TNF-α* mRNA expression by MAVS, $MAVS_{S442A}$, and $MAVS_{E457D}$, but not by $MAVS_{K461R}$, was significantly inhibited by ORF7b (Fig. 3C through E). The results suggested that MAVS Lys461 was essential for the inhibition of the MAVS-mediated RLR signal pathway by ORF7b.

$MAVS_{K461}$/K63 ubiquitination was essential for the RLR signaling regulated by the MAVS–ORF7b complex

It has been shown that K63 polyubiquitin chains are required to activate MAVS and RIG-I (34, 35). To investigate whether MAVS K63 ubiquitination mediated the repression of the RLR signaling pathway by ORF7b, we transfected HEK293T cells and HEK293T-ORF7b-GFP cells with MAVS and ubiquitin (wild type [WT], K48, K63) expression plasmids, and then infected the cells with Sendai virus. We determined the *IFN-β*, *IFITM3*, and *TNF-α* mRNA levels with qPCR. The results showed that *IFN-β*, *IFITM3*, and *TNF-α* mRNA levels were significantly increased by MAVS and ubiquitin WT overexpression. The increases were inhibited by ORF7b as expected (Fig. 4A through C). Compared with the control, overexpression of ubiquitin WT, K48, and K63 resulted significant increases in the *IFN-β*, *IFITM3*, and *TNF-α* mRNA levels (Fig. 4A through C), suggesting that ubiquitin WT, K48, and K63 were involved in the regulation of *IFN-β*, *IFITM3*, and *TNF-α* mRNA expression by MAVS and ORF7b. Compared with the ubiquitin WT, overexpression of ubiquitin K48 resulted in decreases, and overexpression of ubiquitin K63 resulted in increases in the *IFN-β*, *IFITM3*, and *TNF-α* mRNA expression (Fig. 4A through C). These results suggested that ubiquitin K63 was more involved, and K48 was less involved in the regulation of *IFN-β*, *IFITM3*, and *TNF-α* mRNA expression by MAVS and ORF7b.

K63-linked polyubiquitination of MAVS Lys461 facilitates the formation of prion-like MAVS aggregates (33). To investigate the role of MAVS Lys461 in the physical association between MAVS and ORF7b, we transfected HEK293T cells and HEK293T-ORF7b-GFP cells with ORF7b, MAVS or $MAVS_{K461R}$, and ubiquitin K63 expression plasmids, treated the cells with poly (I:C), and performed co-IP assays. The results showed that overexpression of ubiquitin K63 resulted in a dramatic K63-linked polyubiquitination and reduction in the association between MAVS and ORF7b. Overexpression of ubiquitin K63 resulted in a more dramatic K63-linked polyubiquitination and reduction in the association between $MAVS_{K461R}$ and ORF7b (Fig. 4D). The results suggested that K63-linked polyubiquitination inhibited the association between MAVS and ORF7b. MAVS Lys461 was essential in the inhibition of the association between MAVS and ORF7b by K63-linked polyubiquitination.

The E3 ubiquitinase catalyzes K63-mediated ubiquitination at MAVS and results in the activation of the MAVS, following the phosphorylation of TBK1 and downstream IRF3, and IKKα/β and downstream NF-κB, which in turn result in the induction of IFN-β and TNF-α, respectively (13–15). To investigate the role of MAVS Lys461 in the activation of TBK1, IRF3, and IKKα/β by MAVS and in the regulation by ORF7b and ubiquitin K63, we

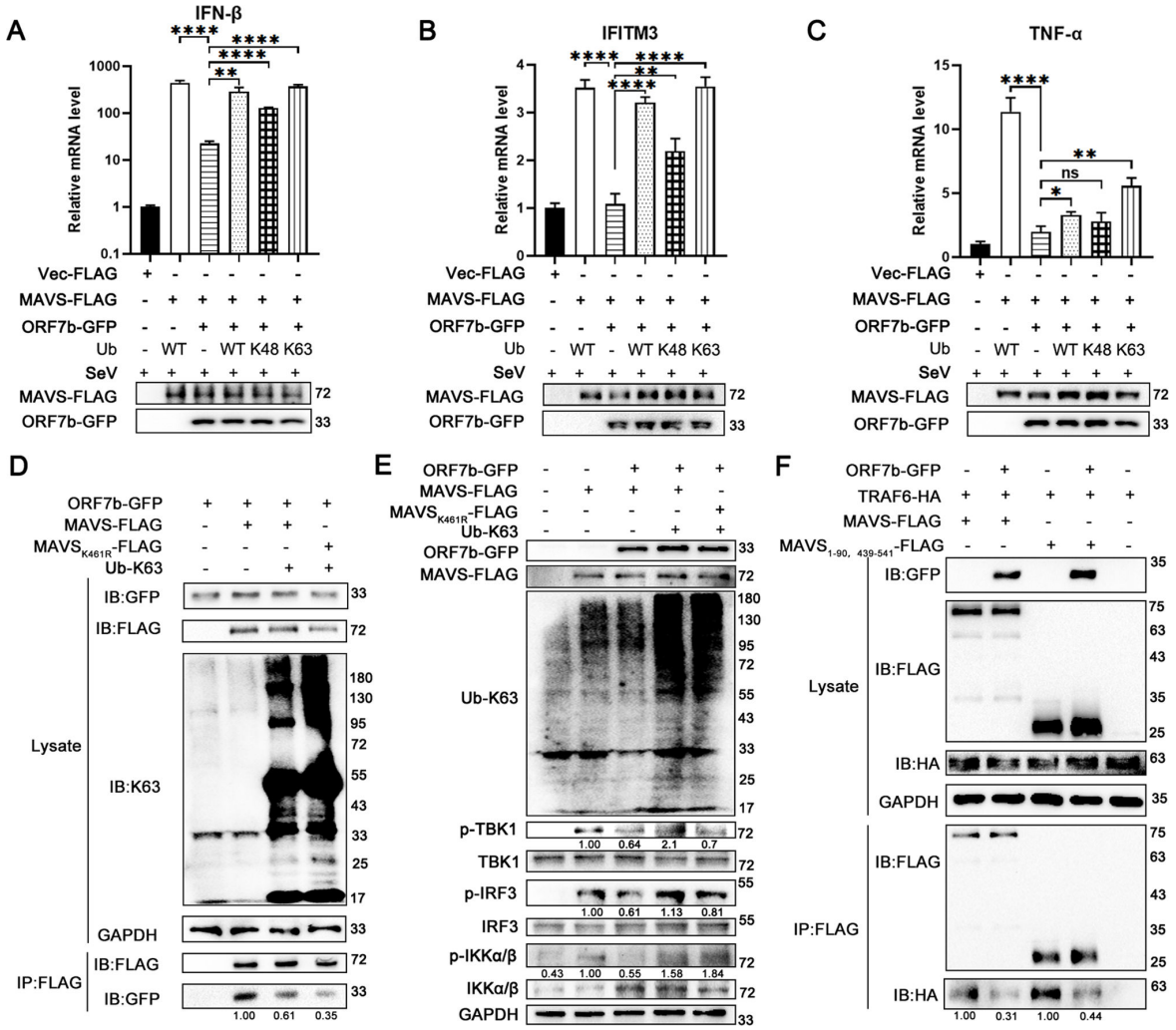

FIG 4 MAVS$_{K461}$/K63 ubiquitination was essential for the RLR signaling regulated by the MAVS–ORF7b complex. (A–C) Ubiquitin K63 was more involved and K48 was less involved in the regulation of *IFN-β*, *IFITM3*, and *TNF-α* mRNA expression by MAVS and ORF7b. HEK293T cells and HEK293T-ORF7b-GFP cells were transfected with MAVS and ubiquitin (WT, K48, K63) expression plasmids for 18 h, and then infected with Sendai virus for 6 h. *IFN-β*, *IFITM3*, and *TNF-α* mRNA levels in the cells were determined using qPCR. (D) MAVS K461 was essential in the inhibition of the association between MAVS and ORF7b, and regulated K63-linked polyubiquitination. The HEK293T cells and HEK293T-ORF7b-GFP cells were transfected with ORF7b, MAVS or MAVS$_{K461R}$, and ubiquitin K63 expression plasmids for 18 h, and then treated with 10 µg/mL poly (I:C) for 6 h. Co-IP assays were performed. (E) MAVS K461 was essential in the regulation of TBK1, IRF3, and IKKα/β by ORF7b and MAVS as well as K63-linked polyubiquitination. The HEK293T cells and HEK293T-ORF7b-GFP cells were transfected with ORF7b, MAVS or MAVS$_{K461R}$, and ubiquitin K63 expression plasmids for 18 h, and then treated with 10 µg/mL poly (I:C) for 6 h. The total and the phosphorylated protein levels of TBK1, IRF3, and IKKα/β were determined using Western blotting. (F) ORF7b inhibited the interaction between TRAF6 and MAVS. The HEK293T cells and HEK293T-ORF7b-GFP cells were transfected with TRAF6, ORF7b, MAVS, or MAVS$_{1-90,439-541}$ expression plasmids for 18 h, and then treated with 10 µg/mL poly (I:C) for 6 h. Co-IP assays were performed. *$P < 0.05$, **$<I>P < 0.01$, and ***$<I>P < 0.001$; ns, no significant difference compared with the MAVS plus ORF7b and Ub-WT group (one-way ANOVA and Tukey's post-hoc test). ****$</>P < 0.0001$.

transfected HEK293T cells and HEK293T-ORF7b-GFP cells with ORF7b, MAVS or MAVS$_{K461R}$, and ubiquitin K63 expression plasmids, and then treated the cells with poly (I:C). We determined the total and the phosphorylated protein levels of TBK1, IRF3, and IKKα/β using Western blotting. The results showed that overexpression of ORF7b resulted in reduction in the phosphorylated protein levels but not in the total protein levels of TBK1 and IRF3, and reduction in the phosphorylated protein level and increases in the total protein level of IKKα/β in the HEK293T cells overexpressing MAVS (Fig. 4E). Overexpression of ubiquitin K63 resulted in significant increases in K63-linked polyubiquitination and increases in the phosphorylated protein levels but not in the total protein levels

of TBK1, IRF3, and IKKα/β regulated by MAVS and ORF7b (Fig. 4E). Compared with those of wild-type MAVS, the phosphorylated protein levels but not the total protein levels of TBK1 and IRF3 were significantly decreased, the phosphorylated protein level of IKKα/β was significantly increased, and the total protein level of IKKα/β was decreased by $MAVS_{K461R}$ (Fig. 4E). These results suggested that K63-linked polyubiquitination was involved in the regulation of TBK1, IRF3, and IKKα/β by ORF7b and MAVS. MAVS Lys461 was essential in the regulation of TBK1, IRF3, and IKKα/β by ORF7b and MAVS.

TRAF6 is required for MAVS signaling complex to activate IKK and TBK1 (13). To investigate the effect of ORF7b on the interaction between TRAF6 and MAVS, we transfected HEK293T cells and HEK293T-ORF7b-GFP cells with TRAF6, ORF7b, MAVS, or $MAVS_{1\text{-}90,439\text{-}541}$ expression plasmids, treated the cells with poly (I:C), and performed co-IP assay. The results showed that overexpression of ORF7b resulted in decreases in the amount of immune-precipitated TRAF6 by MAVS or $MAVS_{1\text{-}90,439\text{-}541}$ (Fig. 4F). The results suggested that ORF7b inhibited the interaction between TRAF6 and MAVS. Furthermore, these results suggested that $MAVS_{K461}$/K63 ubiquitination was essential for the RLR signaling regulated by the MAVS–ORF7b complex. ORF7b interfered with the recruitment of downstream component TRAF6 and the activation of the RLR signaling pathway by MAVS.

Interfering peptides targeted the ORF7b tetramer and reversed the suppression of the MAVS-mediated RLR signaling pathway by ORF7b

ORF7b was predicted to be a transmembrane protein (Fig. S1). It has been speculated that the SARS-CoV-2 ORF7b protein may form homotetramers with ion channel activity (36, 37). To examine whether ORF7b forms tetramers in cells, we resolved the lysate of cells overexpressing ORF7b-GFP using tricine SDS-denatured PAGE and tricine incomplete-denatured PAGE, and probed with an anti-GFP antibody. The results showed that the ORF7b-GFP band was located along with the 33kD marker resolved in the tricine SDS-denatured PAGE (Fig. 5A), suggesting that the molecular weight of ORF7b-GFP was around 33 kD. Consistently, there was an ORF7b-GFP band along with the 33kD marker in the tricine incomplete-denatured PAGE. Furthermore, there was a broader ORF7b-GFP band located around the 130kD marker in the tricine incomplete-denatured PAGE (Fig. 5B). The results suggested ORF7b-GFP formed tetramers in cells. A tetramer model of SARS-CoV-2 ORF7b was generated from the GalaxyWEB server (38) and I-TASSER server (39). The ORF7b tetramer possessed an N-terminal, a transmembrane domain that may insert into the mitochondrial membrane, and a C-terminal random coli exposed outside (Fig. 5C). The interaction model of ORF7b and MAVS oligomers generated using the HDOCK SERVER showed that $ORF7b_{30\text{-}36}$ was essential for the interaction with amino acid residues 442, 443, 461 to 463 of MAVS (Fig. S2; Table S1).

Interfering peptides are promising drug candidates to disrupt protein–protein interactions (PPIs) and target intracellular molecules (40). To prevent ORF7b from repressing MAVS-mediated innate immune response (27), we designed several interfering peptides (IntPep I–V) according to the interaction model of ORF7b and MAVS oligomers. These peptides contained ORF7b-homologous sequences involved in the interaction between MAVS and ORF7b tetramers, contained HIV-TAT in the C-terminal of peptides to facilitate the entrance of the interfering peptides into cells (41, 42), and were biotin-labeled (Fig. 5D). These peptides entered the cells (Fig. S3A and B) and exhibited minimal cytotoxicity at doses below 50 µM (Fig. S3C).

To examine the effects of IntPep I–V on the MAVS-activated RLR signaling pathway, we transfected HEK293T cells and HEK293T-ORF7b-GFP cells with IFN-β-pGL3, MAVS-FLAG expression plasmids, and the control plasmid (pCMV-Flag), followed by poly (I:C) and IntPep I–V treatment. We then determined the relative luciferase activity. The results showed that the ORF7b/MAVS-regulated IFN-β promoter activity was significantly increased by IntPeps I, II, III, and V but not by IntPep IV. The magnitude of increase by IntPep V was the biggest (Fig. 5E). Similar results were observed in the *IFN-β*, *IFITM3*, and *TNF-α* mRNA levels in the HEK293T-ORF7b-GFP cells transfected with MAVS-FLAG

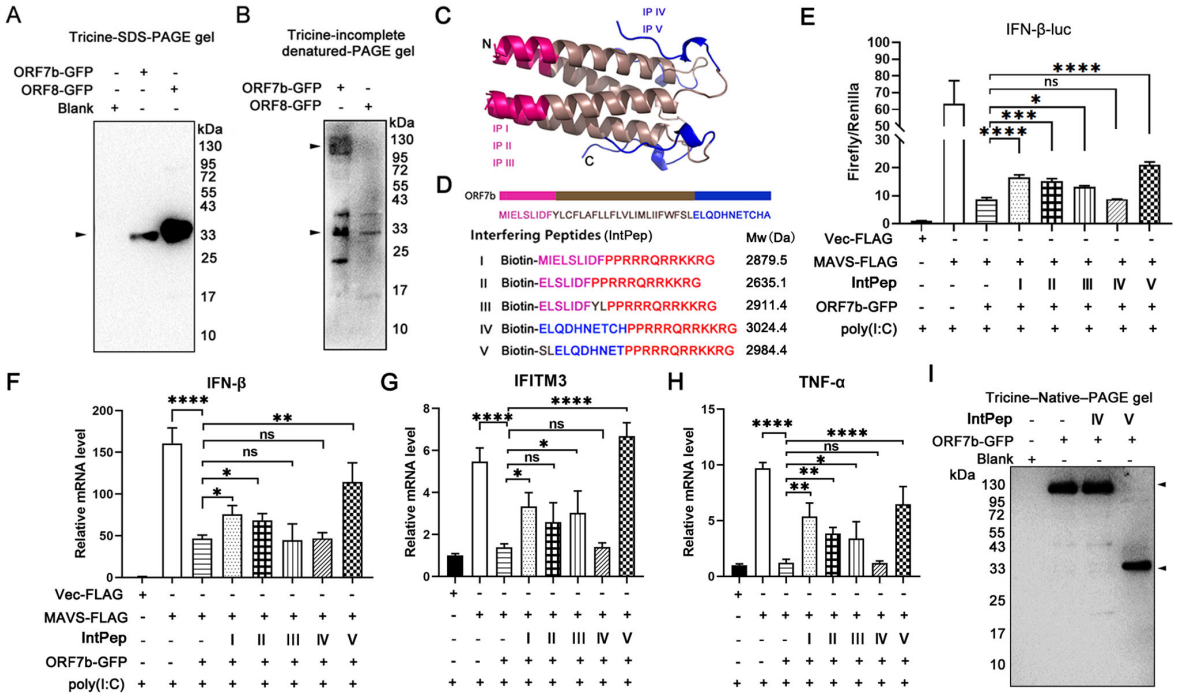

FIG 5 Interfering peptides targeted the ORF7b tetramer and reversed the suppression of the MAVS-mediated RLR signaling pathway by ORF7b. (A, B) ORF7b–GFP formed a tetramer in cells. The lysate of HEK293T cells expressing ORF7b-GFP was separated by tricine SDS-PAGE (A) or tricine incomplete-denatured-PAGE (B). Arrows indicate the tetramer and monomer. Cells expressing ORF8-GFP were set as a control group (B). (C) ORF7b tetramer was obtained from the GalaxyWEB server (38) and I-TASSER server (39). (D) IntPep I–V was designed to block the interaction between ORF7b and MAVS. The peptides were biotin-labeled and contained ORF7b-homologous sequences and C-terminal HIV-TAT sequences. (E) Interfering peptides reversed the ORF7b-suppressed IFN-β promoter activity activated by MAVS. HEK293T cells and HEK293T-ORF7b-GFP cells were transfected with IFN-β-pGL3, MAVS-FLAG expression plasmids, and the control plasmid (pCMV-Flag) for 18 h, followed by 10 µg/mL poly (I:C) and 50 µM IntPep I–V treatment for 6 h. The relative luciferase activity in cells was determined. (F–H) Interfering peptides reversed the ORF7b-suppressed *IFN-β*, *IFITM3*, and *TNF-α* mRNA levels activated by MAVS in the HEK293T cells. The HEK293T cells and HEK293T-ORF7b-GFP cells were transfected with the MAVS-FLAG expression plasmids and the control plasmid (pCMV-Flag) for 18 h, followed by 10 µg/mL poly (I:C) and 50 µM IntPep I–V treatment for 6 h. The *IFN-β*, *IFITM3*, and *TNF-α* mRNA in cells were determined using qPCR. (I) IntPep V but not IntPep IV prevented the formation of ORF7b tetramer in the HEK293T cells. The HEK293T-ORF7b-GFP cells were treated with 50 µM IntPeps for 6 h. The cell lysate was resolved in a tricine-native PAGE. Arrows indicate the tetramer and monomer. **P* < 0.05, ***P* < 0.01, ****P* < 0.001, and *****P* < 0.0001; ns, no significant difference compared with the MAVS plus ORF7b group (one-way ANOVA and Tukey's post-hoc test).

expression plasmids (Fig. 5F through H). These results suggested that interfering peptides reversed the suppression of the MAVS-mediated RLR signaling pathway by ORF7b.

To examine whether IntPep V interferes with the formation of ORF7b tetramer, we resolved the lysate of HEK293T-ORF7b-GFP cells treated with IntPeps IV or V using tricine non-denatured PAGE, and probed with an anti-GFP antibody. The results showed that there was only one major band along with the 130kD marker in the lanes loaded with samples from the groups with the vehicle and IntPep IV treatments. There was only one major band along with the 33kD marker in the lane loaded with the sample from the group with the IntPep V treatment (Fig. 5I). The results suggested that IntPep V but not IntPep IV prevented the formation of ORF7b tetramer in the HEK293T cells.

Interfering peptide V reversed the levels of the ORF7b-inhibited physical association between MAVS and TRAF6, and suppressed viral infection and growth

To examine the effects of IntPep V on the association between ORF7b and MAVS, we transfected HEK293T-ORF7b-GFP cells with MAVS expression plasmids, treated the cells with poly (I:C) and IntPep IV or V, and performed co-IP assays. The results showed that

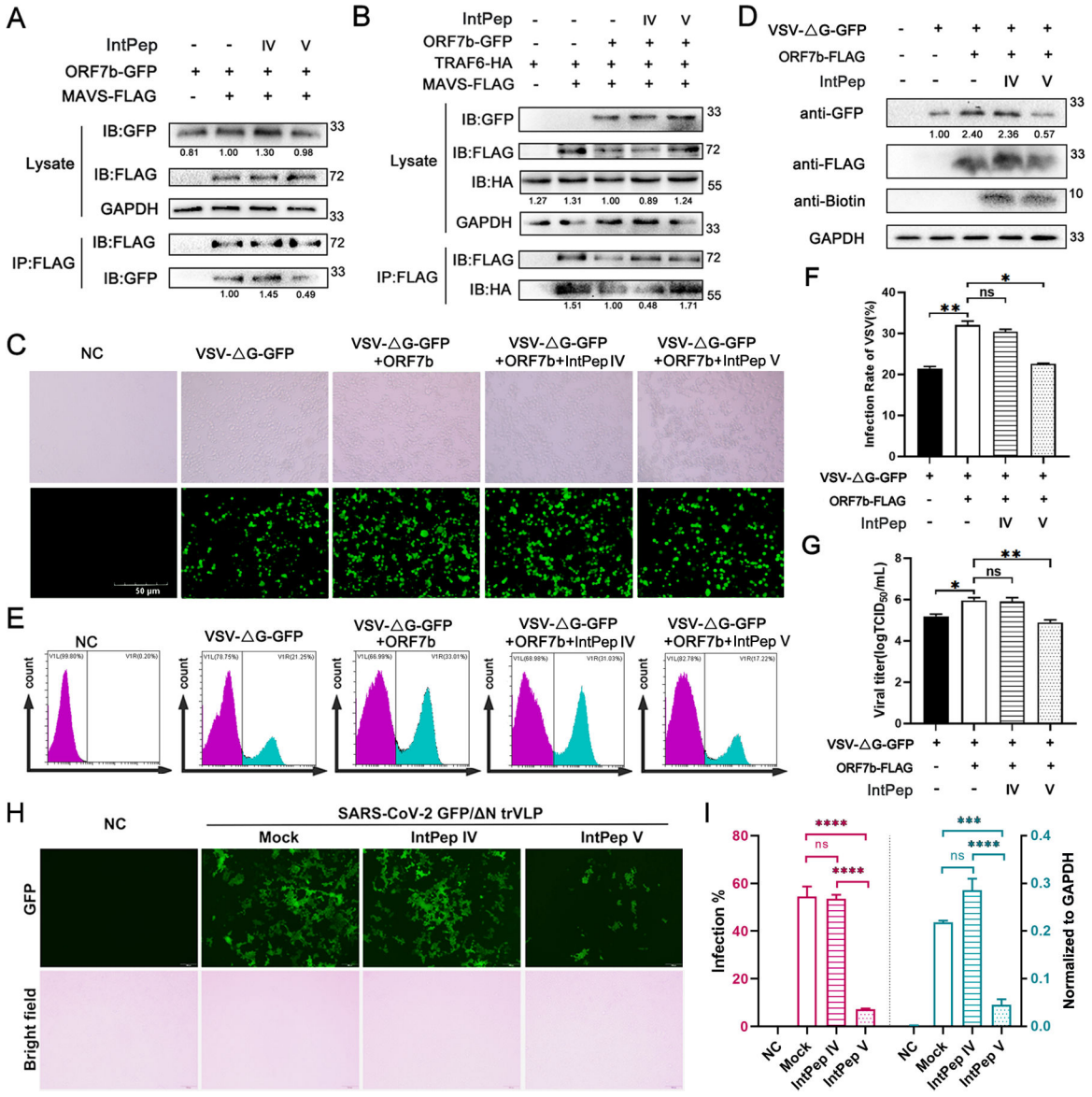

FIG 6 Interfering peptide V reversed the levels of the ORF7b-inhibited physical association between MAVS and TRAF6, and suppressed viral production and infection. (A) IntPep V but not IntPep IV dramatically inhibited the physical association between ORF7b and MAVS. HEK293T-ORF7b-GFP cells were transfected with MAVS-FLAG expression plasmids for 18 h and treated with 10 μg/mL poly (I:C) and 50 μM IntPep (IV, V) for 6 h. Co-IP assays were performed. (B) IntPep V reversed the levels of the ORF7b-inhibited physical association between MAVS and TRAF6. HEK293T cells and HEK293T-ORF7b-GFP cells were transfected with MAVS-FLAG and TRAF6-HA expression plasmids for 18 h, and treated with 10 μg/mL poly (I:C) and 50 μM IntPep (IV, V) for 6 h. Co-IP assays were performed. (C-G) IntPep IV suppressed the viral production and infection of viral VSV-ΔG-GFP in the HEK293T cells. The HEK293T cells were co-transfected with pCAGGS-ORF7b-FLAG or pCAGGS plasmids and pMD2G. Eighteen hours later, the cells were treated with 50 μM IntPep (IV, V) for 6 h and then infected with VSV-ΔG-GFP for 12 h. The cells and media were subjected to subsequent examination. (C, D) IntPep V but not IntPep IV dramatically suppressed VSV-ΔG-GFP production. GFP expression was observed and photographed using a fluorescence microscopy (C) and was determined using Western blotting (D). (E, F) IntPep V treatment resulted in decreases in the rate of GFP-positive HEK293T cells. The GFP-positive cells were identified using flow cytometry assay (E). Infection rate was calculated according to the result of the flow cytometry assays (F). (G) The viral VSV-ΔG-GFP titer was significantly decreased by IntPep V. Viral titers in the media were determined using the Spearman-Karber method. (H, I) IntPep V treatment resulted in an inhibited growth and infection rate of SARS-CoV-2 GFP/ΔN trVLP in Caco-2-N cells. The Caco-2-N cells expressing viral nucleocapsid were treated with 50 μM IntPep (IV, V) for 6 h and then infected with SARS-CoV-2 trVLP at an MOI of 1 for 1 h. After 24 h, the cells were examined using fluorescence microscopy (H). Infection rates were calculated in triplicate based on the intensity of GFP fluorescence quantified using the software Image J (I, left panel). Relative viral subgenomic RNA levels normalized to *GAPDH* were determined by RT-qPCR analysis (I, right). *$P < 0.05$, **$P < 0.01$, ***$P < 0.001$, and ****$P < 0.0001$; ns, no significant difference, one-way ANOVA and Tukey's post-hoc test. NC, negative control.

IntPep V but not IntPep IV dramatically inhibited the physical association between ORF7b and MAVS (Fig. 6A). To examine the effects of IntPep V on the association between ORF7b and MAVS, we transfected HEK293T cells and HEK293T-ORF7b-GFP cells with MAVS and TRAF6-HA expression plasmids, treated the cells with poly (I:C) and IntPep IV or IntPep V, and performed co-IP assays. The results showed that IntPep V allowed the interaction between MAVS and TRAF6 by inhibiting the ORF7b binding to MAVS (Fig. 6B).

To investigate the effect of IntPep V on the viral infection and production, we transfected HEK293T cells with pCAGGS-ORF7b-FLAG or empty vector (pCAGGS) and pMD2G, treated cells with IntPep IV or IntPep V, and then infected the cells with VSV-ΔG-GFP and determined infection and production of VSV-ΔG-GFP. The results showed that GFP was expressed in HEK293T cells infected with VSV-ΔG-GFP as determined by fluorescence microscopy (Fig. 6C) and Western blotting (Fig. 6D), suggesting that the production of viral VSV-ΔG-GFP was present in HEK293T cells. IntPep V but not IntPep IV dramatically suppressed VSV-ΔG-GFP production, compared with the control (Fig. 6C and D). Further, the flow cytometry results confirmed the presence of GFP positive HEK293T cells after VSV-ΔG-GFP infection (Fig. 6E) and showed that IntPep V treatment resulted in decreases in the rate of GFP positive HEK293T cells, compared with the control (Fig. 6E and F). The viral VSV-ΔG-GFP titer was significantly decreased by IntPep V but not IntPep IV (Fig. 6G).

We further used a transcription and replication-competent SARS-CoV-2 virus-like-particles (trVLP) system expressing GFP reporter gene to examine the effect of IntPep V on growth of SARS-CoV-2 (43). The results showed that IntPep V but not IntPep IV treatment resulted in a dramatically lower infection rate and viral RNA level of SARS-CoV-2 trVLP (Fig. 6H and I). These results suggested that IntPep V suppressed the viral infection and growth, indicating a potential therapeutic agent for SARS-CoV-2.

DISCUSSION

SARS-CoV-2 infection results in the compromise of the innate immunity (7, 10, 21, 44, 45). The tumor necrosis factor alpha pathway and the production of IFN-β are blocked by ORF7b (24, 25). In the current study, we found that ORF7b facilitates viral infection and production, and inhibits the RLR signaling pathway through selectively interacting with MAVS. $MAVS_{439\text{-}466}$ region and MAVS Lys461 are essential for the physical association between MAVS and ORF7b, and the inhibition of the RLR signaling pathway by ORF7b. $MAVS_{K461}$/K63 ubiquitination is essential for the RLR signaling regulated by the MAVS–ORF7b complex. ORF7b interferes with the recruitment of TRAF6 and activation of the RLR signaling pathway by MAVS. Furthermore, we have identified interfering peptides that target the ORF7b complex and reverse the ORF7b-suppressed RLR signaling pathway activated by MAVS. Among them, the most potent interfering peptide V disrupts the formation of ORF7b tetramers, reverses the levels of the ORF7b-inhibited physical association between MAVS and TRAF6, and suppresses viral production and infection. Overall, our study likely provides a mechanism for the compromised innate immunity by SARS-CoV-2 infection and the mechanism-based approach via interfering peptides to potentially prevent SARS-CoV-2 infection and production (Fig. 7).

MAVS plays an important role in antiviral infection and is a central adaptor for activating downstream antiviral genes (46–48). SARS-CoV-2 has developed immune evasion strategies to degrade or block the proteins involved in the RLR receptor signaling pathway. Upon SARS-CoV-2 infection, the membrane glycoprotein M interacts with MAVS, impairing MAVS aggregation and its recruitment of downstream TRAF3, TBK1, and IRF3, leading to attenuation of the innate antiviral response (49). ORF9b protein inhibits the IFN-I pathway by interacting with MAVS and preventing the phosphorylation and nuclear translocation of IRF3 (17). ORF9b also inhibits the binding between hTOM70 and Hsp90, which undermines the recruitment of Hsp90 to TBK1/IRF3, thus weakening the signaling cascade for the IFN-I pathway (18, 19). ORF10 inhibits the IFN-I pathway by inducing mitophagy-mediated degradation of MAVS (20). In the current study, we found that ORF7b facilitates viral infection and production, and inhibits the RLR signaling

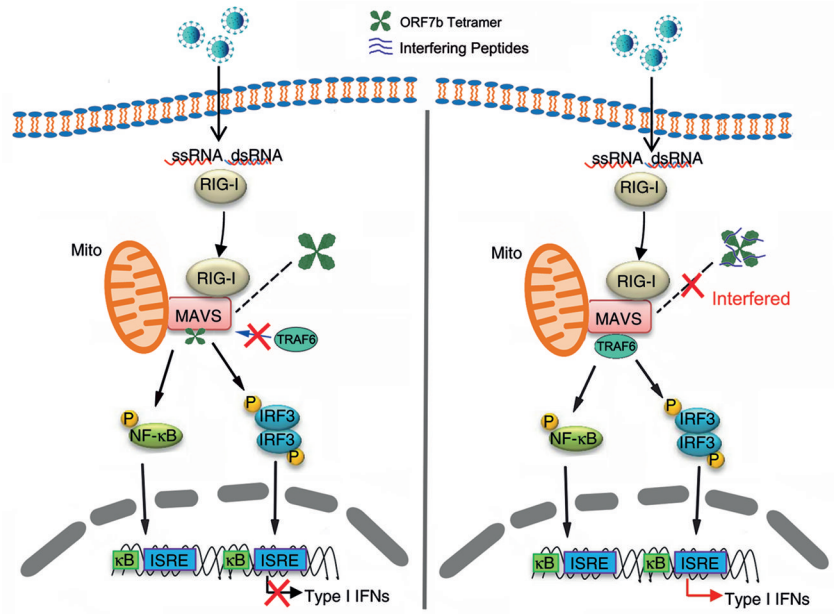

FIG 7 Schematic model of reversion of ORF7b-mediated suppression of the RLR signaling pathway upon SARS-CoV-2 infection by interfering peptides. After infection, SARS-CoV-2 dsRNA was recognized by pattern recognition receptors, and RIG-I-like receptor signal pathway was activated. MAVS recruits TRAF6 to induce the transcription of IFN-β and proinflammatory cytokines. ORF7b interacts with MAVS and then inhibits the K63-linked ubiquitination, thereby disturbing the production of proinflammatory cytokines and IFN-β (left). The interfering peptide inhibits the interaction between ORF7b and MAVS, rescuing the recruitment of TRAF6 to MAVS and boosting the RIG-I signaling pathway (right).

pathway through selectively interacting with MAVS. $MAVS_{439-466}$ region and MAVS Lys461 are essential for the physical association between MAVS and ORF7b, and the inhibition of the RLR signal pathway by ORF7b. ORF7b also interferes with the recruitment of TRAF6 and activation of the RLR signaling pathway by MAVS. This likely provides another MAVS-mediated mechanism for the compromise of the host innate immunity by SARS-CoV-2 infection.

In the current study, the results of co-IP assays support that the $MAVS_{439-466}$ domain is required for MAVS to interact with ORF7b. This is consistent with the confocal microscopy results. We speculate that this may be related to the CARD domain and TM domain of MAVS, which facilitates the formation of prion-like MAVS aggregates (50), and the C-terminal TM domain, which locates MAVS on the outer mitochondrial membrane (51). $MAVS_{1-180}$ and $MAVS_{1-438}$ do not have the TM domain. It may be difficult for them to localize to the outer mitochondrial membrane but recruits endogenous MAVS to form prion-like aggregates, resulting in co-localization with ORF7b.

The signaling adaptor MAVS requires Lys63 (K63)-linked polyubiquitin chains to initiate the type I interferon signaling (52). Ubiquitin E3 ligase interacts with MAVS and catalyzes the K63-linked polyubiquitination of Lys461 on MAVS, which promotes the formation of prion-like aggregates of MAVS after viral infection and activation of antiviral signaling pathways (33). SARS-CoV-2 can target K63 ubiquitination to inhibit host organism immune responses (53). In this study, we found that ubiquitin K63 is more involved and K48 is less involved in the regulation of *IFN-β*, *IFITM3*, and *TNF-α* mRNA expression by MAVS and ORF7b. K63-linked polyubiquitination inhibits the association between MAVS and ORF7b. MAVS Lys461 is essential not only for the physical association between MAVS and ORF7b and the inhibition of the expression of *IFN-β*, *IFITM3*, and *TNF-α* by ORF7b, but also in the inhibition of the association between MAVS and ORF7b by K63-linked polyubiquitination. It is likely that $MAVS_{K461}$/K63 ubiquitination is essential

for the RLR signaling regulated by the MAVS–ORF7b complex, supporting the role and the mechanism of MAVS in mediating ORF7b-suppressed RLR signaling.

Targeting disease-relevant protein–protein interactions is a promising strategy to develop peptide drugs (26), as evidenced by interfering peptides that target the SARS-CoV-2 nuclear coat protein dimer structure to disrupt the liquid–liquid phase separation of SARS-CoV-2-NP, thereby enhancing the intrinsic antiviral response of the host *in vitro* and *in vivo* (27). In the current study, we found ORF7b-GFP forms tetramers in cells. This is consistent with the studies by Toft-Bertelsen et al. and Surya et al. that ORF7b may form homotetramers to act as a viroporin ion channel (36, 37). The interaction model of ORF7b and MAVS oligomers indicates that $ORF7b_{30\text{-}36}$ and the amino acid residues 442, 443, 461 to 463 of MAVS are involved in the interaction. This is consistent with the experimental data. The short peptides containing the ORF7b-homologous sequence and HIV-TAT and biotin enter the cells and exhibit minimal cytotoxicity. They reverse the ORF7b-suppressed RLR signaling pathway activated by MAVS. The most potent $ORF7b_{31\text{-}40}$ -homologous interfering peptide disrupts the ORF7b tetramer and reverses the suppression of the MAVS-mediated RLR signaling pathway by ORF7b, as well as reverses the levels of the ORF7b-inhibited physical association between MAVS and TRAF6 and suppresses viral production and infection. The offset of two residues in IntPep V may reduce the positive charge and increase the hydrophilicity, resulting in a suppression effect. Therefore, interfering peptide V may provide a potential way to prevent SARS-CoV-2 infection and viral production.

In conclusion, ORF7b inhibits the RLR signaling pathway through the physical association between ORF7b and MAVS, impairing the K63-linked MAVS polyubiquitination and its recruitment of TRAF6 to MAVS. The most potent interfering peptide V targeting the ORF7b–MAVS complex may reverse the suppression of the MAVS-mediated RLR signaling pathway by ORF7b and prevent viral infection and growth of SARS-CoV-2. This study may provide new insights into the pathogenic mechanism of SARS-CoV-2 and a strategy to develop new drugs to prevent SARS-CoV-2 infection.

MATERIALS AND METHODS

Construction of plasmids

The recombinant plasmids express wild-type or mutated MAVS-FLAG, and TRAF6-HA, ORF7b-FLAG, and ORF7b-GFP were constructed using PCR cloning. The coding sequences of human genes *MAVS* (GenBank: KC415005.1) and *TRAF6* (GenBank: U78798.2), and the viral gene *ORF7b* (GenBank: NC_045512.2) (NCBI) (https://www.ncbi.nlm.nih.gov/) were used as the templates to construct plasmids using PCR cloning. The cDNA fragment of *MAVS* was amplified using the forward primer 5′- *GCTTG GTACCATGCCGTTTGCTG*-3′ and the reverse primer 5′- *TAATCTCGAGCTAGTGCAGAC*-3′ with the added restriction endonucleases sites *Kpn*I and *Xho*I/*Xba*I, respectively. The cDNA fragment of *TRAF6* was amplified using 5′-*CCGGAATTCTGATGAGTCTGCTAAACTGTG*-3′ and 5′-*AATGGTACCGTTACCCCTGCATCAGTACTTC*-3′ with the added restriction endonucleases sites *Eco*RI and *Kpn*I, respectively. The cDNA fragment of *ORF7b* was amplified using the forward primer 5′-*TGGCCTCGAGATGATTGAACTTTCATTAATTG*-3′ and the reverse primer 5′-*TAATCCGCGGGGCGTGACAAGTTTCATTATG*-3′ with the added restriction endonucleases sites *Xho*I and *Sac*II, respectively, the forward primer 5′-*TGGCGAATTCATGATTGAACTTTCAT TAATTG*-3′ and the reverse primer 5′-*TAATGGTACCGGCGTGACAAGTTTCATTATG*-3′ with the added restriction endonucleases sites *Eco*RI and *Kpn*I, respectively. The PCR fragments were modified using respective restriction endonucleases and were inserted into the vectors pCAGGS-HA, pCAGGS-Flag, and pWPXLd-GFP. All plasmids were amplified using DH5α *Escherichia coli*. Positive clones were screened using PCR and were verified by DNA sequencing. Plasmids pCMV-RIGI-Flag (P39598), pCMV-MDA5-Flag (P22743), and pCMV-TBK1-Flag (P45111) were purchased from MiaoLing Bio Ltd (Wuhan, China).

Cell culture and treatment

HEK293T, Caco-2-N, and HEK293T-ORF7b-GFP cells, which stably expressed ORF7b-GFP, were cultured in Dulbecco's Modified Eagle's Medium (DMEM) supplemented with 10% heat-inactivated fetal bovine serum (FBS) and 1% penicillin–streptomycin at 37°C in a 5% CO_2 incubator. The cells in the logarithmic phase were digested with 0.25% trypsin (Basal Media, S310JV) and were seeded at a density of 50,000/well into 12-well plates or 10^6 cells into 10-cm dishes. After incubation for 24 h, the cultured cells were transfected with expression plasmids using Lipofectamine 6000 Reagent (Beyotime, C0526) by following the manufacturer's instructions and/or were treated with interfering peptides for 12 h, infected with VSV-ΔG-GFP for 1 h, and then incubated with virus maintenance media for 12 h. These cells were collected and used for flow cytometry assay and Western blotting analysis.

Preparation of virus and evaluation of antiviral activity

VSV-ΔGFP and vector pMD2G were transferred from Prof. Guiqing Peng's lab in Huazhong Agricultural University (Wuhan, China). SARS-CoV-2 GFP/ΔN trVLP and Caco-2-N cell lines were obtained from Prof. Qiang Ding in Tsinghua University (Beijing, China). Caco-2-N cells expressing viral nucleocapsid were infected with SARS-CoV-2 trVLP at an multiplicity of infection(MOI) of 1 for 1 h, washed three times with phosphate-buffered saline (PBS), and incubated in 2% FBS culture medium for 24 h for fluorescence observation and viral subgenomic RNA determination. The SARS-CoV-2 trVLP cell culture system was used in a BSL-2 facility of Hubei University of Medicine (Shiyan, Hubei, China).

HEK293T cells were seeded into 10-cm dishes at a density of 10^6 cells per dish and were cultured overnight. The cells were transfected with pMD2G plasmid. After washing with PBS, the cells were incubated with VSV-ΔGFP at 37°C for 1 h and then incubated with High Glucose DMEM media (Gibco, C11960500BT) containing 2% FBS and 1% penicillin–streptomycin for 36–72 h. The cells were collected by centrifugation at 1,000 rpm for 10 min in a desktop high-speed freezing centrifuge (Eppendorf, 5424R) to obtain VSV-ΔG-GFP.

After the HEK293T cells were transfected with related plasmids for 24 h or treated with interfering peptides, the cells were infected with VSV-ΔG-GFP for 1 h and then incubated for 12 h with virus maintenance media. Then, the supernatant of infected cells was collected to determine the virus titer. To determine the $TCID_{50}$ of the supernatant from different groups, samples were serially diluted from 10^{-3} to 10^{-8}. After the cells were seeded in 96-well plates and grown in the logarithmic phase, washing with PBS and 100-µL supernatant diluted with DMEM were added. Each dilution was repeated five times. After 72-h infection, the cells were examined, and the virus titer was calculated using the Spearman-Karber method (54).

Determination of the viral infection rate

The HEK293T cells were infected with viral VSV-ΔG-GFP and were subjected to a flow cytometry assay using a CytoFLEX system (Beckman Coulter). The ratio between the amount of HEK293T cells expressing GFP and the amount of total HEK293T cells was calculated. Each experiment was performed in triplicate. Caco-2-N cells were infected with SARS-CoV-2 GFP/ΔN trVLP, and the GFP-positive cells were observed by a Fluorescence Microscopy (Olympus, FV3000RS). The infection rates were calculated based on the intensity of GFP fluorescence quantified using the software Image J. The relative viral subgenomic RNA levels of SARS-CoV-2 GFP/ΔN trVLP normalized to *GAPDH* were determined using real-time (RT)-qPCR analysis.

Western blotting analysis

Cells were lysed with the RIPA lysis buffer (50 mM Tris-HCl, 150 mM NaCl, 1% NP-40, and 100 µM PMSF, pH 7.4). The protein concentrations of all samples were determined using BCA Protein Quantitative Kit (Absin, abs9232).

To resolve proteins in denatured SDS-PAGE, an aliquot of 10-µg protein of each sample was incubated with 5× SDS loading buffer, boiled in a 100°C metal bath for 10 min, and then resolved in SDS-PAGE with SDS-containing buffer. To resolve proteins in incomplete-denatured PAGE gels, an aliquot of 10-µg protein of each sample was mixed with 5× non-denature loading buffer (Beyotime, P0292) and then resolved in incomplete-denatured PAGE gels with the SDS-containing buffer. To resolve proteins in non-denatured PAGE gels, an aliquot of 10-µg protein of each sample was mixed with 5× non-denature loading buffer (Beyotime, P0292) and then resolved in non-denatured PAGE gels with the SDS-free buffer.

After electrophoresis, proteins were transferred to the polyvinylidene difluoride (PVDF) membranes (Millipore, ISEQ00005). The PVDF membranes were blocked with 5% skimmed milk dissolved in TBST buffer at room temperature for 1 h and then incubated with a primary antibody overnight at 4°C. After washing with TBST five times, the membranes were incubated with a horseradish peroxidase-coupled secondary antibody for 3 h at 4°C. After washing with TBST five times, the membranes were incubated with enhanced chemiluminescence (ECL) reagents (Beyotime, P0018FM). The signals were recorded using a gel imaging analyzer (Bio-Rad, 721BR11621) and were analyzed using the Image Lab software (BioRad). The antibodies included rabbit polyclonal anti-HA (Santa Cruz, sc-805, 1:2,000), mouse monoclonal anti-FLAG (M2, Sigma-Aldrich, F1804, 1:2,000), rabbit polyclonal anti-GAPDH (Proteintech, 10494-1-AP, 1:2,000), HRP-mouse anti-biotin (Invitrogen, 03-3720, 1:1,000), rabbit polyclonal anti-GFP (Proteintech, 50430-2-AP, 1:2,000), HRP-conjugated secondary antibodies goat anti-mouse IgG (H+L) (1:5,000, Proteintech, SA00001-1), and goat anti-rabbit IgG (H+L) (1:5,000, Proteintech, SA00001-2).

Luciferase-based IFN-β reporter assay

HEK293T cells and HEK293T-ORF7b-GFP cells were seeded in 12-well plates at a density of 50,000 cells/well and were cultured overnight. The cells were co-transfected with the reporter plasmids of pIFN-β-pGL3 (Addgene#102597) and pRL-SV40 (Addgene#27163) and overexpression plasmids using Lipofectamine 6000 (Beyotime, C0526) by following the manufacturer's protocol, and then treated with 10 µg/mL poly (I:C) for 6 h. The cells were lysed using 1× passive lysis buffer (Promega, E1910) for 15 min. The Firefly and Renilla luciferase activities of the lysates were measured using relevant reagents (Promega, E1910) on a SpectraMax i3x microplate reader (Molecular Devices, Afghanistan) according to the manufacturer's instructions. Experiments were performed in triplicate.

Co-IP assay

HEK293T cells and HEK293T-ORF7b-GFP cells were seeded at a density of 10^6 cells into 10-cm dishes and were cultured overnight. The cells were co-transfected with the plasmids expressing MAVS/$MAVS_{1\text{-}90,439\text{-}541}$, TRAF6 or Ub-K63 using Lipofectamine 6000 (Beyotime, C0526) by following the manufacturer's protocol, and then treated with 10 µg/mL poly (I:C) for 6 h. After culture for 24 h, the cells were harvested and lysed in 600-µL RIPA lysis buffer (50 mM Tris-HCl, 150 mM NaCl, 1% NP-40, and 100 µM PMSF, pH 7.4). The lysates were centrifuged at 20,000 *g* at 4°C for 10 min. An aliquot of 500-µL cell lysates was incubated with the anti-FLAG antibody coupled with magnetic beads overnight at 4°C. The magnetic beads were precipitated using a magnetic block, washed with PBST at room temperature five times, and eluted with glycine-HCl (pH2.5). The elutes were collected, neutralized using Tris-HCl (pH 8.8), and then subjected to Western blotting analysis.

Reverse transcription-quantitative PCR

Total RNAs were extracted from the cells using TRIzol reagent (Thermo Fisher Scientific, 15596026) according to the manufacturer's instructions. Complementary DNA (cDNA) was synthesized using HiScript III RT SuperMix for qPCR reagent (Vazyme, R323-01). qPCR was set up using Taq Pro Universal SYBR qPCR Master Mix reagent (Vazyme, Q712-02) in a 20-µL scale. The PCR was run on a CFX96 Real-Time PCR Detection System (BioRad) by following the program 95°C 3 min, 95°C 10 s, 55°C 30 s (39 cycles), and 65°C 5 s. The *GAPDH* gene was used as an internal reference, and all reactions were performed in triplicate. The mRNA levels of target genes were calculated using the $2^{-\triangle\triangle Ct}$ method (55). The primers are listed in Table S2.

Immunocytochemistry assay and confocal microscopy

HEK293T and HEK293T-ORF7b-GFP cells at a density of 5,000 cells/well were seeded into 12-well plates where glass slides coated with 0.1% gelatin were placed and cultured overnight. Plasmids expressing MAVS or its truncates were co-transfected in the cells using Lipofectamine 6000 (Beyotime, C0526) by following the manufacturer's protocol. After 24 h, the cells were washed with PBS and fixed with cell fixative (Solarbio, P1111) for 15 min. The cells were washed five times with 0.2% (wt/vol) Triton X-100 in TBS (TBST-X) for 5 min each at room temperature. Then, the cells were blocked with PBS containing 5% FBS for 3 h. After three times of TBST-X washing, the samples were incubated with the primary antibody (anti-FLAG [M2], Sigma-Aldrich, F1804, 1:200) overnight at 4°C. After washing, cells were incubated with the secondary antibody conjugated with Alexa Fluor 488 or Alexa Fluor 555 for 3 h. Then, the cells were washed five times. Finally, confocal slides were placed on glass slides containing mounting medium (DAPI, Invitrogen, D1306). The cells were observed and photographed using confocal microscopy (Nikon, PCM-2000). The PCC between 0.5 and 1.0 indicating the two co-localized fluorescence signals (30) was analyzed using the Image J 1.0 software.

Designing and screening interfering peptides

The overlapping peptides containing the ORF7b-homologous sequences were designed according to the previous report (56). The N-terminal of interfering peptides was conjugated with a biotin tag, and the C-terminal contained an HIV-TAT transmembrane sequence (42). The interfering peptides were manufactured by Yuanpeptide Co. Ltd. (Nanjing) in 5-µg scale at >99% purity and were stored at −20°C in powder. For *in vitro* experiments, the powder was dissolved in PBS to generate a 50-mM stock and avoid repeat freeze-thaw.

Data analysis

Data analysis was performed using GraphPad Prism 8.0.2. Data are shown with mean ± SD from three independent experiments. In addition, significant differences among groups were determined using one-way analysis of variance (ANOVA) or Student's *t*-test. $P < 0.05$ was considered significant.

ACKNOWLEDGMENTS

We thank Dr. Qiang Ding of Tsinghua University for kindly providing the SARS-CoV-2 trVLP system. We are also thankful to Prof. Yu Chen of Wuhan University and Prof. Guiqing Peng of Huazhong Agricultural University for their technical support.

This research was supported by the National Natural Science Foundation of China (82002149), the Natural Science Foundation of Hubei Province (2022CFB451), the Principal Investigator Program at Hubei University of Medicine (HBMUPI202102), the Foundation of Health Commission of Hubei Province (WJ2021M059), and the Innovative Research Program for Graduates of Hubei University of Medicine (YC 2023016). The

funders had no role in the study design, data collection, or preparation of the manuscript.

Conceptualization: G.C., Z.X.L., W.X.D., and L.L. Supervision: Z.X.L. and L.L. Data collection: X.X., Y.N.F., W.L.Y., F.Z., and C.C.H. Investigation and methodology: Y.N.F., W.L.Y., F.Z., C.C.H., X.G.S., and J.L. Resources: G.C., Q.W.Z., and W.X.D. Writing and editing the manuscript: X.X., X.S.G., G.C., and L.L.

AUTHOR AFFILIATIONS

[1]Department of Infectious Diseases, Renmin Hospital, School of Basic Medical Sciences, Hubei University of Medicine, Shiyan, China
[2]Institute of Virology, Shiyan Key Laboratory of Virology, Hubei University of Medicine, Shiyan, China
[3]Hubei Key Laboratory of Embryonic Stem Cell Research, Hubei University of Medicine, Shiyan, China
[4]Guangdong Provincial Key Laboratory of Virology, Institute of Medical Microbiology, Jinan University, Guangzhou, China
[5]New Cornerstone Science Laboratory, Tsinghua-Peking Joint Center for Life Sciences, School of Basic Medical Sciences, Tsinghua University, Beijing, China

AUTHOR ORCIDs

Jian Li http://orcid.org/0000-0001-9434-7803
Qiwei Zhang http://orcid.org/0000-0002-2770-111X
Gong Cheng http://orcid.org/0000-0001-7447-5488
Zhixin Liu http://orcid.org/0000-0001-7253-7438
Long Liu http://orcid.org/0000-0002-1265-7603

FUNDING

Funder	Grant(s)	Author(s)
MOST | National Natural Science Foundation of China (NSFC)	82002149	Long Liu

DATA AVAILABILITY

The data that support the findings of this study are available from the corresponding authors upon reasonable request.

ADDITIONAL FILES

The following material is available online.

Supplemental Material

Supplemental material (JVI01573-23-s0001.docx). Figures S1 to S3; Tables S1 and S2.

REFERENCES

1. Sharma A, Tiwari S, Deb MK, Marty JL. 2020. Severe acute respiratory syndrome coronavirus-2 (SARS-CoV-2): a global pandemic and treatment strategies. Int J Antimicrob Agents 56:106054. https://doi.org/10.1016/j.ijantimicag.2020.106054
2. Li Q, Guan X, Wu P, Wang X, Zhou L, Tong Y, Ren R, Leung KSM, Lau EHY, Wong JY, et al. 2020. Early transmission dynamics in Wuhan, China, of novel coronavirus-infected pneumonia. N Engl J Med 382:1199–1207. https://doi.org/10.1056/NEJMoa2001316
3. Rodriguez-Morales AJ, Bonilla-Aldana DK, Balbin-Ramon GJ, Rabaan AA, Sah R, Paniz-Mondolfi A, Pagliano P, Esposito S. 2020. History is repeating itself: probable zoonotic spillover as the cause of the 2019 novel coronavirus epidemic. Infez Med 28:3–5.
4. Wu A, Peng Y, Huang B, Ding X, Wang X, Niu P, Meng J, Zhu Z, Zhang Z, Wang J, Sheng J, Quan L, Xia Z, Tan W, Cheng G, Jiang T. 2020. Genome composition and divergence of the novel Coronavirus (2019-nCoV) originating in China. Cell Host Microbe 27:325–328. https://doi.org/10.1016/j.chom.2020.02.001
5. Beacon TH, Delcuve GP, Davie JR. 2021. Epigenetic regulation of ACE2, the receptor of the SARS-CoV-2 virus. Genome 64:386–399. https://doi.org/10.1139/gen-2020-0124
6. Kumar B, Hawkins GM, Kicmal T, Qing E, Timm E, Gallagher T. 2021. Assembly and entry of severe acute respiratory syndrome coronavirus 2 (SARS-CoV2): evaluation using virus-like particles. Cells 10:853. https://doi.org/10.3390/cells10040853
7. Hadjadj J, Yatim N, Barnabei L, Corneau A, Boussier J, Smith N, Péré H, Charbit B, Bondet V, Chenevier-Gobeaux C, et al. 2020. Impaired type I interferon activity and inflammatory responses in severe COVID-19 patients. Science 369:718–724. https://doi.org/10.1126/science.abc6027

8. Hassan SS, Choudhury PP, Dayhoff GW, Aljabali AAA, Uhal BD, Lundstrom K, Rezaei N, Pizzol D, Adadi P, Lal A, et al. 2022. The importance of accessory protein variants in the pathogenicity of SARS-CoV-2. Arch Biochem Biophys 717:109124. https://doi.org/10.1016/j.abb.2022.109124
9. Martino E, Chiarugi S, Margheriti F, Garau G. 2021. Mapping, structure and modulation of PPI. Front Chem 9:718405. https://doi.org/10.3389/fchem.2021.718405
10. Blanco-Melo D, Nilsson-Payant BE, Liu W-C, Uhl S, Hoagland D, Møller R, Jordan TX, Oishi K, Panis M, Sachs D, Wang TT, Schwartz RE, Lim JK, Albrecht RA, tenOever BR. 2020. Imbalanced host response to SARS-CoV-2 drives development of COVID-19. Cell 181:1036–1045. https://doi.org/10.1016/j.cell.2020.04.026
11. Stetson DB, Medzhitov R. 2006. Type I Interferons in host defense. Immunity 25:373–381. https://doi.org/10.1016/j.immuni.2006.08.007
12. Peisley A, Wu B, Xu H, Chen ZJ, Hur S. 2014. Structural basis for ubiquitin-mediated antiviral signal activation by RIG-I. Nature 509:110–114. https://doi.org/10.1038/nature13140
13. Liu S, Chen J, Cai X, Wu J, Chen X, Wu YT, Sun L, Chen ZJ. 2013. MAVS recruits multiple ubiquitin E3 ligases to activate antiviral signaling cascades. Elife 2:e00785. https://doi.org/10.7554/eLife.00785
14. Loo YM, Gale M. 2011. Immune signaling by RIG-I-like receptors. Immunity 34:680–692. https://doi.org/10.1016/j.immuni.2011.05.003
15. Takeuchi O, Akira S. 2010. Pattern recognition receptors and inflammation. Cell 140:805–820. https://doi.org/10.1016/j.cell.2010.01.022
16. Shi CS, Qi HY, Boularan C, Huang NN, Abu-Asab M, Shelhamer JH, Kehrl JH. 2014. SARS-coronavirus open reading frame-9b suppresses innate immunity by targeting mitochondria and the MAVS/TRAF3/TRAF6 signalosome. J Immunol 193:3080–3089. https://doi.org/10.4049/jimmunol.1303196
17. Han L, Zhuang MW, Deng J, Zheng Y, Zhang J, Nan ML, Zhang XJ, Gao C, Wang PH. 2021. SARS-CoV-2 ORF9b antagonizes type I and III Interferons by targeting multiple components of the RIG-I/MDA-5-MAVS, TLR3-TRIF, and cGAS-STING signaling pathways. J Med Virol 93:5376–5389. https://doi.org/10.1002/jmv.27050
18. Gao X, Zhu K, Qin B, Olieric V, Wang M, Cui S. 2021. Crystal structure of SARS-CoV-2 ORF9b in complex with human TOM70 suggests unusual virus-host interactions. Nat Commun 12:2843. https://doi.org/10.1038/s41467-021-23118-8
19. Jiang HW, Zhang HN, Meng QF, Xie J, Li Y, Chen H, Zheng YX, Wang XN, Qi H, Zhang J, Wang PH, Han ZG, Tao SC. 2020. SARS-CoV-2 Orf9B suppresses type I interferon responses by targeting TOM70. Cell Mol Immunol 17:998–1000. https://doi.org/10.1038/s41423-020-0514-8
20. Li X, Hou P, Ma W, Wang X, Wang H, Yu Z, Chang H, Wang T, Jin S, Wang X, Wang W, Zhao Y, Zhao Y, Xu C, Ma X, Gao Y, He H. 2022. SARS-CoV-2 ORF10 suppresses the antiviral innate immune response by degrading MAVS through mitophagy. Cell Mol Immunol 19:67–78. https://doi.org/10.1038/s41423-021-00807-4
21. Singh KK, Chaubey G, Chen JY, Suravajhala P. 2020. Decoding SARS-CoV-2 hijacking of host mitochondria in COVID-19 pathogenesis. Am J Physiol Cell Physiol 319:C258–C267. https://doi.org/10.1152/ajpcell.00224.2020
22. Wang J, Li Z, Xu L, Yang H, Liu W. 2018. Transmembrane domain dependent inhibitory function of FcγRIIB. Protein Cell 9:1004–1012. https://doi.org/10.1007/s13238-018-0509-8
23. Fogeron M-L, Montserret R, Zehnder J, Nguyen M-H, Dujardin M, Brigandat L, Cole L, Ninot-Pedrosa M, Lecoq L, Meier BH, Böckmann A. 2021. SARS-CoV-2 ORF7b: is a bat virus protein homologue a major cause of COVID-19 symptoms? bioRxiv. https://doi.org/10.1101/2021.02.05.428650
24. Shemesh M, Aktepe TE, Deerain JM, McAuley JL, Audsley MD, David CT, Purcell DFJ, Urin V, Hartmann R, Moseley GW, Mackenzie JM, Schreiber G, Harari D. 2021. SARS-CoV-2 suppresses IFNβ production mediated by NSP1, 5, 6, 15, ORF6 and ORF7b but does not suppress the effects of added interferon. PLoS Pathog 17:e1009800. https://doi.org/10.1371/journal.ppat.1009800
25. Yang R, Zhao Q, Rao J, Zeng F, Yuan S, Ji M, Sun X, Li J, Yang J, Cui J, Jin Z, Liu L, Liu Z. 2021. SARS-CoV-2 accessory protein ORF7b mediates tumor necrosis factor-α-induced apoptosis in cells. Front Microbiol 12:654709. https://doi.org/10.3389/fmicb.2021.654709
26. Sorolla A, Wang E, Golden E, Duffy C, Henriques ST, Redfern AD, Blancafort P. 2020. Precision medicine by designer interference peptides: applications in oncology and molecular therapeutics. Oncogene 39:1167–1184. https://doi.org/10.1038/s41388-019-1056-3
27. Wang S, Dai T, Qin Z, Pan T, Chu F, Lou L, Zhang L, Yang B, Huang H, Lu H, Zhou F. 2021. Targeting liquid-liquid phase separation of SARS-CoV-2 nucleocapsid protein promotes innate antiviral immunity by elevating MAVS activity. Nat Cell Biol 23:718–732. https://doi.org/10.1038/s41556-021-00710-0
28. Stukalov A, Girault V, Grass V, Karayel O, Bergant V, Urban C, Haas DA, Huang Y, Oubraham L, Wang A, et al. 2021. Multilevel proteomics reveals host perturbations by SARS-CoV-2 and SARS-CoV. Nature 594:246–252. https://doi.org/10.1038/s41586-021-03493-4
29. Ren Z, Ding T, Zuo Z, Xu Z, Deng J, Wei Z. 2020. Regulation of MAVS expression and signaling function in the antiviral innate immune response. Front Immunol 11:1030. https://doi.org/10.3389/fimmu.2020.01030
30. Mohapatra S, Weisshaar JC. 2018. Modified pearson correlation coefficient for two-color imaging in spherocylindrical cells. BMC Bioinformatics 19:428. https://doi.org/10.1186/s12859-018-2444-3
31. Liu S, Cai X, Wu J, Cong Q, Chen X, Li T, Du F, Ren J, Wu YT, Grishin NV, Chen ZJ. 2015. Phosphorylation of innate immune adaptor proteins MAVS, STING, and TRIF induces IRF3 activation. Science 347:aaa2630. https://doi.org/10.1126/science.aaa2630
32. Xu LG, Wang YY, Han KJ, Li LY, Zhai Z, Shu HB. 2005. VISA is an adapter protein required for virus-triggered IFN-β signaling. Mol Cell 19:727–740. https://doi.org/10.1016/j.molcel.2005.08.014
33. Liu B, Zhang M, Chu H, Zhang H, Wu H, Song G, Wang P, Zhao K, Hou J, Wang X, Zhang L, Gao C. 2017. The ubiquitin E3 ligase TRIM31 promotes aggregation and activation of the signaling adaptor MAVS through Lys63-linked polyubiquitination. Nat Immunol 18:214–224. https://doi.org/10.1038/ni.3641
34. Zeng W, Sun L, Jiang X, Chen X, Hou F, Adhikari A, Xu M, Chen ZJ. 2010. Reconstitution of the RIG-I pathway reveals a signaling role of unanchored polyubiquitin chains in innate immunity. Cell 141:315–330. https://doi.org/10.1016/j.cell.2010.03.029
35. Hou F, Sun L, Zheng H, Skaug B, Jiang QX, Chen ZJ. 2011. MAVS forms functional prion-like aggregates to activate and propagate antiviral innate immune response. Cell 146:448–461. https://doi.org/10.1016/j.cell.2011.06.041
36. Surya W, Queralt-Martin M, Mu Y, Aguilella VM, Torres J. 2022. SARS-CoV-2 accessory protein 7b forms homotetramers in detergent. Virol J 19:193. https://doi.org/10.1186/s12985-022-01920-0
37. Toft-Bertelsen TL, Jeppesen MG, Tzortzini E, Xue K, Giller K, Becker S, Mujezinovic A, Bentzen BH, B. Andreas L, Kolocouris A, Kledal TN, Rosenkilde MM. 2021. Amantadine inhibits known and novel ion channels encoded by SARS-CoV-2 *in vitro*. Commun Biol 4:1347. https://doi.org/10.1038/s42003-021-02866-9
38. Ko J, Park H, Heo L, Seok C. 2012. GalaxyWEB server for protein structure prediction and refinement. Nucleic Acids Res 40:W294–W297. https://doi.org/10.1093/nar/gks493
39. Yang J, Zhang Y. 2015. I-TASSER server: new development for protein structure and function predictions. Nucleic Acids Res 43:W174–W181. https://doi.org/10.1093/nar/gkv342
40. Chang YS, Graves B, Guerlavais V, Tovar C, Packman K, To K-H, Olson KA, Kesavan K, Gangurde P, Mukherjee A, et al. 2013. Stapled α-helical peptide drug development: a potent dual inhibitor of MDM2 and MDMX for p53-dependent cancer therapy. Proc Natl Acad Sci U S A 110:E3445–E3454. https://doi.org/10.1073/pnas.1303002110
41. Baar MP, Brandt RMC, Putavet DA, Klein JDD, Derks KWJ, Bourgeois BRM, Stryeck S, Rijksen Y, van Willigenburg H, Feijtel DA, van der Pluijm I, Essers J, van Cappellen WA, van IJcken WF, Houtsmuller AB, Pothof J, de Bruin RWF, Madl T, Hoeijmakers JHJ, Campisi J, de Keizer PLJ. 2017. Targeted apoptosis of senescent cells restores tissue homeostasis in response to chemotoxicity and aging. Cell 169:132–147. https://doi.org/10.1016/j.cell.2017.02.031
42. Quan X, Sun D, Zhou J. 2019. Molecular mechanism of HIV-1 TAT peptide and its conjugated gold nanoparticles translocating across lipid membranes. Phys Chem Chem Phys 21:10300–10310. https://doi.org/10.1039/c9cp01543d

43. Ju X, Zhu Y, Wang Y, Li J, Zhang J, Gong M, Ren W, Li S, Zhong J, Zhang L, Zhang QC, Zhang R, Ding Q. 2021. A novel cell culture system modeling the SARS-CoV-2 life cycle. PLOS Pathog 17:e1009439. https://doi.org/10.1371/journal.ppat.1009439
44. Ren Y, Shu T, Wu D, Mu J, Wang C, Huang M, Han Y, Zhang XY, Zhou W, Qiu Y, Zhou X. 2020. The ORF3a protein of SARS-CoV-2 induces apoptosis in cells. Cell Mol Immunol 17:881–883. https://doi.org/10.1038/s41423-020-0485-9
45. Miorin L, Kehrer T, Sanchez-Aparicio MT, Zhang K, Cohen P, Patel RS, Cupic A, Makio T, Mei M, Moreno E, et al. 2020. SARS-CoV-2 Orf6 hijacks Nup98 to block STAT nuclear import and antagonize interferon signaling. Proc Natl Acad Sci U S A 117:28344–28354. https://doi.org/10.1073/pnas.2016650117
46. Yan BR, Zhou L, Hu MM, Li M, Lin H, Yang Y, Wang YY, Shu HB. 2017. PKACs attenuate innate antiviral response by phosphorylating VISA and priming it for MARCH5-mediated degradation. PLoS Pathog 13:e1006648. https://doi.org/10.1371/journal.ppat.1006648
47. Wang YY, Liu LJ, Zhong B, Liu TT, Li Y, Yang Y, Ran Y, Li S, Tien P, Shu HB. 2010. WDR5 is essential for assembly of the VISA-associated signaling complex and virus-triggered IRF3 and NF-κB activation. Proc Natl Acad Sci U S A 107:815–820. https://doi.org/10.1073/pnas.0908967107
48. Mao AP, Li S, Zhong B, Li Y, Yan J, Li Q, Teng C, Shu HB. 2010. Virus-triggered ubiquitination of TRAF3/6 by cIAP1/2 is essential for induction of interferon-β (IFN-β) and cellular antiviral response. J Biol Chem 285:9470–9476. https://doi.org/10.1074/jbc.M109.071043
49. Fu Y-Z, Wang S-Y, Zheng Z-Q, Li W-W, Xu Z-S, Wang Y-Y. 2021. SARS-CoV-2 membrane glycoprotein M antagonizes the MAVS-mediated innate antiviral response. Cell Mol Immunol 18:613–620. https://doi.org/10.1038/s41423-020-00571-x
50. Chen YQ, Shi YH, Wu J, Qi N. 2021. MAVS: a two-sided CARD mediating antiviral innate immune signaling and regulating immune homeostasis. Front Microbiol 12:744348. https://doi.org/10.3389/fmicb.2021.744348
51. Seth RB, Sun L, Ea C-K, Chen ZJ. 2005. Identification and characterization of MAVS, a mitochondrial antiviral signaling protein that activates NF-κB and IRF3. Cell 122:669–682. https://doi.org/10.1016/j.cell.2005.08.012
52. Song B, Chen Y, Liu X, Yuan F, Tan EYJ, Lei Y, Song N, Han Y, Pascal BD, Griffin PR, Luo C, Wu B, Luo D, Zheng J. 2021. Ordered assembly of the cytosolic RNA-sensing MDA5-MAVS signaling complex via binding to unanchored K63-linked poly-ubiquitin chains. Immunity 54:2218–2230. https://doi.org/10.1016/j.immuni.2021.09.008
53. Madiraju C, Novack JP, Reed JC, Matsuzawa SI. 2022. K63 ubiquitination in immune signaling. Trends Immunol 43:148–162. https://doi.org/10.1016/j.it.2021.12.005
54. Miller J, Ulrich R. 2001. On the analysis of psychometric functions: the Spearman-Kärber method. Percept Psychophys 63:1399–1420. https://doi.org/10.3758/bf03194551
55. Livak KJ, Schmittgen TD. 2001. Analysis of relative gene expression data using real-time quantitative PCR and the $2^{-\Delta\Delta C_T}$ method. Methods 25:402–408. https://doi.org/10.1006/meth.2001.1262
56. Xu Y, Wasnik S, Baylink DJ, Berumen EC, Tang X. 2017. Overlapping peptide library to map Qa-1 epitopes in a protein. J Vis Exp:56401. https://doi.org/10.3791/56401